Annelid - a Novel Design for Actuated Robots Inspired by Ringed Worm's Locomotion

Christian Mandel* Udo Frese*
*Department of Mathematics and Computer Science - FB3, University of Bremen, Bremen, Germany

***Abstract*— This paper describes the development of a simulation software that advances the idea of a robotic device inspired by ringed worm's locomotion. Its basic design is made up of an elongated body that is composed of a spring-style skeleton which is coated by a flexible skin. Our principle approach is to choose a shape memory alloy material for the skeleton, resulting in different spring forces exerted by the body under varying temperatures. The overall approach requires the elastic skin to prestress the whole body in its rest position, so that it can spatially extend when thermal energy is induced to the system, and relax when an inbuilt air cooling mechanism dissipates the heat.**

***Index Terms*— simulation, snake-like robot, shape memory alloy**

I. Introduction

Like its biological archetypes, snake-like robots impress with a great variability of locomotion. In contrast to robotic devices based on wheeled, legged, or track-driven designs, their ability to move by rhythmically undulating their elongated body with its small diameter qualifies them for application scenarios in rough terrains with potential needs to trespass gaps and loopholes. Hopkins et al. survey in [5] major snake-like robot designs since the early 1970s that differentiate in their implemented locomotion gate, i.e. lateral undulatory, concertina, sidewinding, and rectilinear progression.

Erkmen et al. have proposed a particularly attractive application for snake-like robots, namely to search for victims in the remains of a collapsed building [4]. A snake-like robot could move through tiny holes and caverns, still negotiate obstacles and gaps much larger. It could also be deployed through a hole drilled into a concrete-slab which is a common practice in urban search and rescue to gain access into the rubble pile. In this particular application power supply, computation, and teleoperation could even be realized externally by letting the snake's tail stay outside the rubble pile, a technique that even proved essential with conventional intervention robots [7].

Technically, most snake robots are realized by a long sequence of joints actuated by geared electrical motors. Compared to its biological counterpart this design appears complicated and somehow not adequate considering the visual appearance of a snake as a moving continuous shape with "infinite" degrees of freedom. This gap triggered our approach to investigate an continuous actuation mechanism that could provide a large number, i.e. "infinitely" many, degrees of freedom.

Our idea is based on a shape memory alloy (SMA) spiral [10], intended as a spring. Due to the SMA-effect the spring expands when heated and can be contracted by an external pretension force when cooled down. Menciassi et al. already proved rectilinear motion capabilities by a $3cm$ long robotic crawler that applies a SMA backbone [6]. Instead of integrating the SMA material as a spine, we imagine a spiral forming the outer skeleton of the robot and being wrapped by an elastic skin enclosing the robot and providing the necessary pretension. By heating or cooling the spring locally, local parts of the robot expand and contract, e.g. generating a peristaltic motion to provide propulsion. By heating or cooling the spring on one side only, the spring should expand or contract on one side only and hence bend. This is the mechanism to steer the robot and to adapt its shape to motion and environment, e.g. the control where it contacts the ground. Figure 1 illustrates this envisioned technical concept.

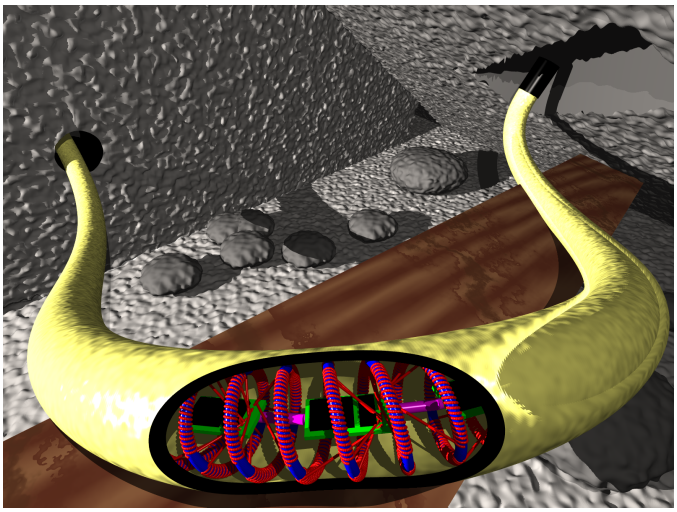

Fig. 1. Illustration of *Annelid* within its envisioned application scenario of a collapsed building. Under the flexible yellow skin, segments of the blue spring-style skeleton, made of shape-memory-alloy (SMA) are covered by red coil-like wires, allowing for thermal heating of parts of the skeleton. The skeleton is cooled by cool air flowing through the core. In doing so, we can control the skeleton's local stiffness by the SMA effect. This leads to an expansion or contraction of the spring and if applied asymmetrically to a bending. Locomotion is realized (in simulation) based on these capabilities. The green boards illustrate the electronics driving the heating coils and being attached to central back-bone wires (magenta) for power supply and control.

We expect the main motion capability to be longitudinal, expanding and contracting the spring, whereas we expect bending to be less effective. Hence, our idea is to imitate the locomotion of ringed worms (cf. Sec. V) who use a longitudinal peristaltic motion, not of snakes who primarily use a bending motion. Further, since ringed worms have a much simpler nervous system compared to snakes we hope

that longitudinal locomotion may be easier to control.

Obviously, technically building such a robot is challenging, in particular concerning the integration of the heating wires, sensors, and electronics in the spring's free inside. So, our first step is to investigate in a detailed simulation whether locomotion is possible given the technical readiness of the system. We report on this investigation here. The paper's two contributions comprise a novel actuation concept for a worm-like robot and a detailed simulation of the robot, covering SMA material behavior including hysteresis, thermal flow for heating and cooling, elasticity of the outer skin, and robot-ground interaction.

The remainder of this paper is structured as follows. In the rest of this section we overview essential properties of SMAs. Sec. II describes the simulation framework used to investigate our design approach. In Sec. III we detail constructional components of the simulated Annelid, i.e. its skeleton, skin, and the heating/cooling approach used. We continue in Sec. IV with a characterization of the implemented austensite martensite hysteresis model, before Sec. V describes our algorithmic approach to control common movement patterns. We conclude in Sec. VI with a summary of the results achieved, and a description of future works that address remaining issues.

A. Shape Memory Alloy

The unique properties of SMA were first observed in 1951 for Au-Cd alloy, and in 1963 for Ti-Ni alloy [9]. Dutta et al. describe the main effect as the alloy's ability to regain its original undeformed state when heated to a high temperature after being deformed at a low temperature [2]. The high temperature Austensite phase (AS), and the low temperature Martensite phase (MS) share the same chemical composition and atomic order, but different crystallographic structures. While AS phases are dominated by highly symmetric structures, MS phases are characterized by low symmetric monoclinic structures [12]. SMAs behaving as described are subject to the so-called *one way memory effect* (OWME). These materials can acquire a *two way memory effect* (TWME) by a cyclic loading procedure called *training* [1]. The TWME shows an additional active transformation during MS phases. Both OWME, and TWME can exert large forces against external resistance, e.g. a NiTi (nickel/titanium) alloy wire of $0.02inch$ diameter can lift up to 16 pounds during its AS phase.

It may be noticed that in recent years ferromagnetic shape memory alloy (FSMA) has triggered various works concentrating on fundamental research [14]. In these alloys the shape-memory effect is triggered by a magnetic field not by temperature. A magnetic field can be switched on and off quickly, allowing for a higher response frequency compared to temperature controlled SMA. So, these materials are expected to allow for new application scenarios in the years to come, and clearly also the approach we present here would benefit from FSMA becoming available.

II. Simulation Overview

Being an intermediate step between the pure idea of an artificial worm-like robotic device, and the construction of a first prototype, *Annelid Simulation* focuses on the interplay of physical forces exerted by Annelid's locomotion mechanism and its surrounding environment. For this purpose we make use of the *NVIDIA PhysX* SDK [8], which provides without limitation the necessary infrastructure for simulating rigid body dynamics, cloth simulation, and collision detection. Beside these available components, we provide additional simulation components that handle thermodynamic calculations for Annelid's skeleton and heating/cooling system, as well as a movement generator that builds upon the distinct effects of annelid's shape memory alloy made skeleton (including martensite-austensite-hysteresis effects).

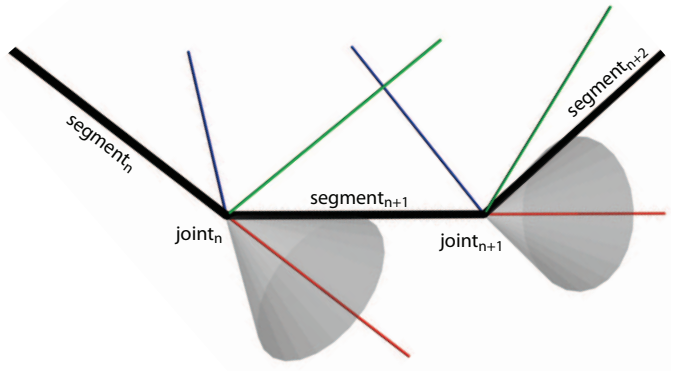

Fig. 2. Illustration of single segments from Annelid's spring-like skeleton. Two consecutive segments are interconnected by a restricted 6DOF joint, depicted by the joint's coordinate frame. While all translational degrees of freedom, as well as the rotation around the joint's y-axis (green) and z-axis(blue) are locked, $segment_{n+1}$ can rotate (twist) around the x-axis (red) of $joint_n$, hereby inducing a restoring force within the joint. Twisting of this joint in the simulation corresponds to torsion of the SMA wire, which is the main mode of strain encountered in a compression spring.

III. Construction of Simulated Annelid

A. Annelid's Skeleton

We model Annelid's shape giving skeleton by a sequence of capsules, i.e. cylindrical elements with hemispheres at the two ends, that are arranged in form of a common compression spring (cf. Fig. 8 for an illustration, and Table I for morphological and physical parameters of the simulated spring). Two consecutive capsules are connected by a partially restricted 6DOF joint such that a force that is applied to the spring exhibits a usual spring-like behavior of the whole system (cf. Fig. 2 for an illustration). When a capsule twists out of its rest-position around the x-axis of the joint that connects it with its predecessor, it induces a restoring force within this joint. PhysX models this restoring force by a spring force that can be parametrized with appropriate spring-, damping-, and restitution-coefficients. It may be noted that this restoring force is the connecting link between the simulated skeleton and the shape memory alloy's property to exert a certain force that pushes the material to its default shape during AS temperature phases. To be exact, we couple the average thermal energy of two neighboring capsules with the spring force simulated within the connecting joint (cf. Sec. IV).

TABLE I

SUBSET OF INITIAL MORPHOLOGICAL AND PHYSICAL PARAMETERS OF ANNELID'S SKELETON

length along main axis	0.3m
radius	0.04m
number of windings	15
segments/winding	8
wire radius	3.5mm
density	$7440 \frac{kg}{m^3}$
specific heat capacity	$470 \frac{J}{kg*K}$
thermal conductivity coefficient	$42.6 \frac{W}{K*m}$
remissivity coefficient	0.5
austensite start temperature	$362.15° K$
austensite end temperature	$383.15° K$
martensite start temperature	$381.65° K$
martensite end temperature	$360.65° K$

B. Annelid's Skin

Annelid's spring-style skeleton is coated with an elastic skin such that the whole compound forms a tube through which the cooling air can funnel (cf. Sec. III-C). Further reasons for the skin are the sheltering of Annelid's inner electronics that control the heating and cooling system, as well as a prestressing of the skeleton. The later allows for expansion of the skeleton under heating, and contraction in cooling down phases (cf. Sec. IV). We model Annelid's skin by a single PhysX cloth element. Intended to be used for simulating stretchable matter such as clothing material, cloths are represented by a mesh of particles interconnected by springs that mimic constraints between these particles (cf. Fig. 3). Beside general quantities for thickness, density, static and dynamic friction, PhysX cloth elements are described by parameters that model the behavior of the cloth springs. These include bending stiffness, stretching stiffness, and a damping coefficient.

Unfortunately, the current PhysX SDK version 2.8.4 realizes collision detection for cloth elements by solely testing on contact between the cloth particles and other objects, e.g. the ground plane. Future versions are announced to implement cloth collision detection on basis of the triangles that make up the cloth patch. To moderate this inaccuracy we currently disable the collision check of Annelid's skin and get by with a collision test between the skeleton's surface and the ground.

C. Annelid's Heating and Cooling System

The primary locomotion mechanism of Annelid builds upon the temperature sensitive properties of the shape memory alloy made skeleton (cf. Sec. IV). For this reason we have modeled a heating and cooling mechanism that approximates our key ideas that are to be realized in a first physical prototype.

D. Heating System

For heating up chosen parts of the spring-style skeleton we plan to attach coiled filaments to the whole framework (cf. exposed heating wires in Fig. 1). By applying voltage to given sections of this heating elements, ohmic resistance causes the induction of thermal energy into the spring. We modeled this behavior by simply allowing for bringing in

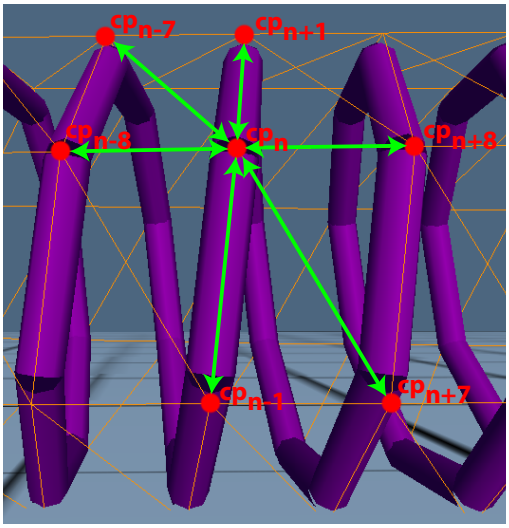

Fig. 3. Illustration of Annelid's elastic skin that is modeled by a single PhysX cloth element. The orange colored cloth element coats the purple colored skeleton and is made up of a mesh structure. An exemplary patch from this cloth mesh is given by red-colored cloth points and green-colored interconnecting springs that provide for the adherence of spatial restrictions between neighboring cloth points.

certain amounts of energy per simulation time step into a single skeleton capsule. A second mechanism is given by the formulation of a list of desired temperatures for the whole list of capsules that make up the skeleton. During operation each capsule's current temperature is measured, and a control loop takes care for maintaining the desired temperature level. Using this approach it is possible to specify and maintain a certain temperature baseline including a systematic description of regions with more/less thermal energy. Being simple to encode in simulation, a real world prototype would require to be equipped with temperature sensors along the whole skeleton.

E. Cooling System

The cooling mechanism of Annelid basically builds on a fan-powered stream of air. For the first real world prototype we envision an ordinary personal computer housing fan with a diameter of $8cm$ and a capacity of $50l/s$ cooling air to be integrated into the tail of Annelid. In order to assess whether this type of cooling mechanism is able to dissipate a sufficient amount of thermal energy per time, we have modeled three physical effects involved [13].

1) Thermal Radiation: The first effect describes the property of each matter to emit electromagnetic radiation, thus loosing thermal energy. In the simulation of Annelid, thermal radiation (1) is one of two effects that account for an exchange of energy between Annelid's skeleton and the cooling air.

$$Q = \varepsilon \cdot \sigma \cdot A \cdot T^4 \cdot \Delta t, \tag{1}$$

with

- $\varepsilon\,[-]$ being the remissivity ranging between 0 for complete reflective materials, and 1 for a true *black body*,
- $\sigma = 5.67 * 10^{-8} \left[\frac{W}{m^2 \cdot K^4}\right]$ being the *Stefan Boltzmann Constant*,

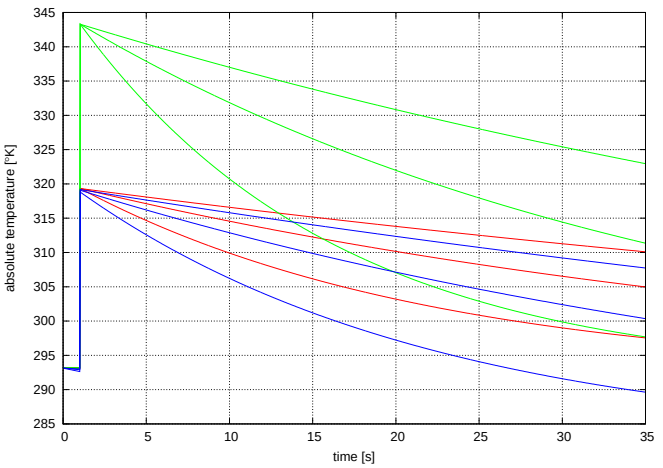

Fig. 4. Cooling behavior of a single segment S from Annelid' skeleton. Each line depicts the temperature over time of S after being heated from $293.15K$ with a thermal energy of $100J$ at $t = 1s$. All of the three temperature-bundles (red, green, blue) differ by the speed of the cooling air, i.e. top:$50l/s$, middle:$150l/s$, and bottom:$500l/s$. The three bundles itself discriminate in the initial exhaust air temperature T, and the radius r of S. It holds: red($T = 293.15K$, $r = 3.5mm$), green($T = 293.15K$, $r = 2.5mm$), and blue($T = 283.15K$, $r = 3.5mm$).

- $A\,[m^2]$ being the body's radiating surface,
- $T\,[K]$ being the body's absolute temperature, and
- $\Delta t\,[s]$ being the observed period of time.

2) Heat Conduction: The second effect is given in (2) and describes the propagation of thermal energy between neighboring skeleton segments with different temperatures at the same time.

$$Q = \lambda \cdot \frac{A}{s} \cdot (T_A - T_B) \cdot \Delta t \tag{2}$$

with

- $\lambda\,\left[\frac{W}{K \cdot m}\right]$ being the coefficient of thermal conductivity,
- $\frac{A}{s}\,\left[\frac{m^2}{m}\right]$ describing the ratio of contact surface and thickness of the matter through which the thermal energy passes,
- $T_A, T_B\,[K, K]$ being the absolute temperatures of the two points between we observe thermal conduction, and
- $\Delta t\,[s]$ being the observed period of time.

3) Thermal Transfer: Just as thermal radiation, the third effect (3) is responsible for an exchange of thermal energy between the skeleton and the cooling air. It is based on the exchange of thermal energy between solid matter and a circulating fluid. Thermal transfer can heat up solid matter or dissipate heat in subject to the given temperature gradient.

$$Q = \alpha \cdot A \cdot (T_A - T_B) \cdot \Delta t, \tag{3}$$

with

- $\alpha\,\left[\frac{W}{K \cdot m^2}\right]$ being the thermal transfer coefficient dependent on the body's surface structure and the fluid's velocity,
- $A\,[m^2]$ being the contact surface between the body and the fluid,
- $T_A, T_B\,[K, K]$ describing the absolute temperatures of the body and the fluid, and
- $\Delta t\,[s]$ being the observed period of time.

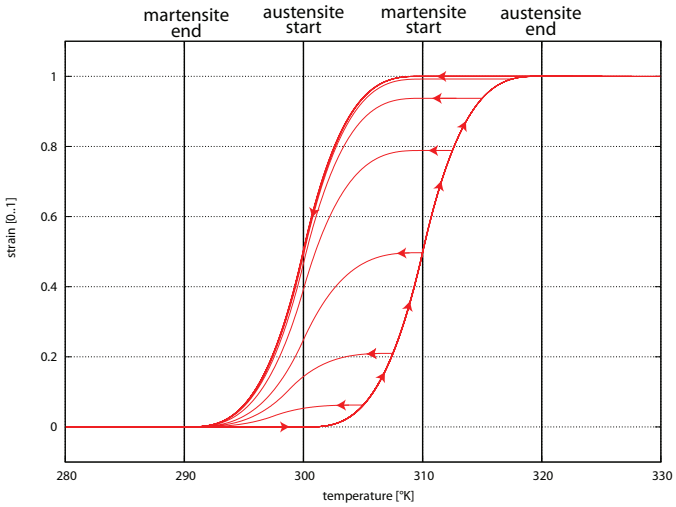

Fig. 5. Simulated austensite-martensite-hysteresis of Annelid's shape memory alloy made skeleton. During the exemplary austensite phase starting at $A_s = 300°K$, and ending at $A_e = 320°K$, the metallic alloy exerts a large force that rearranges the shape of the skeleton towards its stable and stiff state. During the exemplary martensite phase starting at $M_s = 310°K$, and ending at $M_e = 290°$, the material can be deformed by an external force, e.g. by the prestressing force exerted by Annelid's elastic skin. Inner hysteresis loops are reached when temperature decreases before austensite end temperature has been reached, or when temperature increases before martensite end temperature has been reached respectively.

For a given cooling air speed cas we use the textbook formula in [13], namely

$$\alpha = \begin{cases} 5.6 + 4 \cdot cas, & \text{for } cas \leq 5m/s \\ 7.12 \cdot cas^{0.78}, & \text{else} \end{cases} \tag{4}$$

Fig. 4 shows exemplary temperature curves for a single skeleton capsule that is initially heated up by an energy of $100J$, and cooled down according to (1)-(3).

IV. Austensite-Martensite Hysteresis of Simulated Annelid

In Sec. I-A we described the essential properties of shape memory alloys. The most important effect is given by an active strain pushing the material into its original shape during high temperature (AS) phases, and a deformability by external forces during low temperature (MS) phases. This effect turns out to be a non-linear relationship between the material's thermal energy and the internally exerted force. According to [15], it can be modeled as a hysteretic relation with cubic slopes (cf. Fig. 5 for an illustration). For any given fraction of the material's AS/MS workspace, i.e. the interval ranging from *martensite end* to *austensite end* mapped to $T \in [0..1]$, we compute the coefficient $h(T)$ for the resulting force as in (5).

$$h(T) = \begin{cases} 4 \cdot T^3 & : \quad T < 0.5 \\ 1 - 4 \cdot (1 - T)^3 & : \quad T \geq 0.5 \end{cases} \tag{5}$$

V. Locomotion of Simulated Annelid

So far we have described the structural layout of simulated Annelid, its heating and cooling mechanism, as well as the

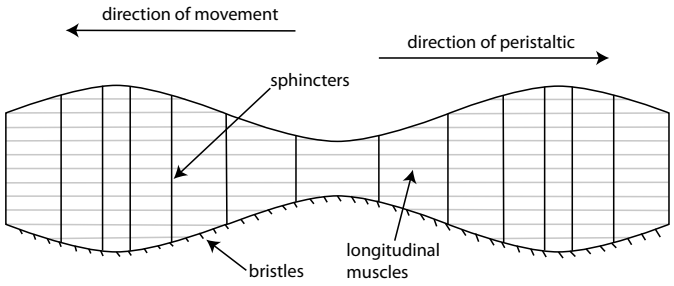

Fig. 6. Illustration of the common earthworms' locomotory system. The depicted shape corresponds to the sagittal plane of an earthworm oriented to the left of the image.

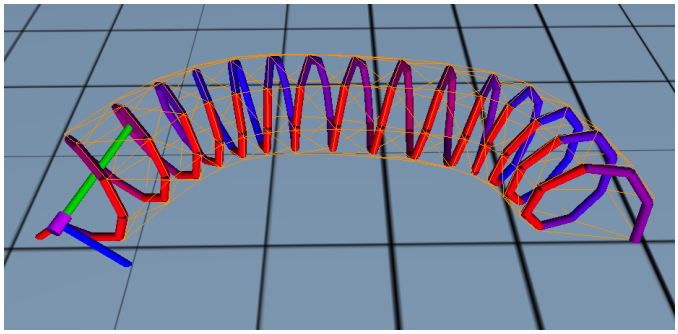

Fig. 7. Illustration of simulated forward movement with superimposed left turn. Annelid's skeleton bends to the left due to the selective heating of left flanking segments.

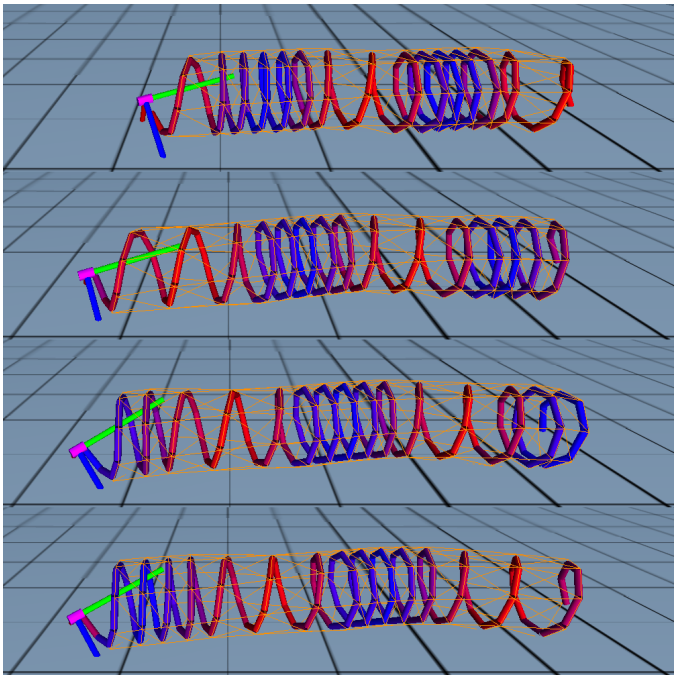

Fig. 8. Illustration of simulated forward movement from $t = 1s$ in top frame, to $t = 2.5s$ in bottom frame. The color of the skeleton segments denotes their actual temperature, ranging from red (high temperature) to blue (low temperature). It can be seen that the actual forward movement (to the left in the images) occurs between frames 1 and 2, where the front segments expand.

shape memory alloy's reaction to varying thermal energy, based on AS/MS hysteresis. In this section we describe the interaction of all components described, resulting in controllable movement of Annelid.

The basic principle of locomotion mimics the movement pattern of the common earthworm, i.e. *Lumbricadae*, a ringed worm of the order *Oligochaeta* within the clade of *Annelida* [3]. Annelida's anatomy can be characterized by several sphincters forming its tubular body, combined with longitudinal muscles (cf. Fig. 6 for an illustration). During basic forward movement, a peristaltic moves into the opposite direction through Annelida's body. This wave provides for alternating body-sections in which sphincters decrease/increase the body's diameter, and longitudinal muscles elongate/contract the body's length. During this process, body segments with increased diameter gain the necessary ground friction through little abdominal bristles.

A. Basic Forward Movement

Inspired by the basic concept of earth worms' forward movement, simulated Annelid's locomotion is driven by a temperature curve that travels in caudal (front $\rightarrow$ back) direction through the body. Windings of the skeleton with higher temperature exert a larger force within joints that connect two consecutive segments, thus stretching subsequent windings and reducing their diameter by the way. Compared with this, windings with lower temperature are contracted, leaving these parts of the spiral with an increased diameter and isolated points of ground contact (cf. Fig. 8 for an illustration). We modeled the initial desired temperature of Annelid's skeleton by a base-temperature of $358°K$ plus a superimposed sinusoidal temperature curve of 4π length. For the chosen simulation parameters as given in Table I, e.g. an initial skeleton length of $0.3m$ with a total of 15 windings $\times$ 8 segments, we add a maximum of $400J/winding$ at the desired temperature curve's peaks. In doing so, the skeleton segments are subject to a temperature interval ranging from $358°K$ up to $376°K$, which corresponds to available SMA operation ranges [11]. Fig. 9 depicts the resulting trajectory from $60s$ of simulated forward movement.

B. Bending - Sidewards Movement

A basic forward movement can change into a turn left/right movement by adding thermal energy to lateral flanking skeleton segments[1] on top of the skeleton's temperature curve necessary for forward movement (as described in the previous subsection). In doing so, simulated Annelid's body bends into the direction of the heated flank (cf. Fig. 7 for an illustration). We calculate the overall desired amount of thermal energy $E_{flankSeg}$ for every flanking segment, such that it equals the maximal desired skeleton segment energy necessary for forward movement, plus a constant δE (6). Fig. 9 shows that a variation of δE results in a changing curvature of the traveled path.

$$E(flankSeg) = max_{i=1}^{|seg|} E(seg_i) + \delta E \qquad (6)$$

[1]A real-world prototype of Annelid has to be equipped with inertial measurement units that indicate the current orientation of the skeleton segments.

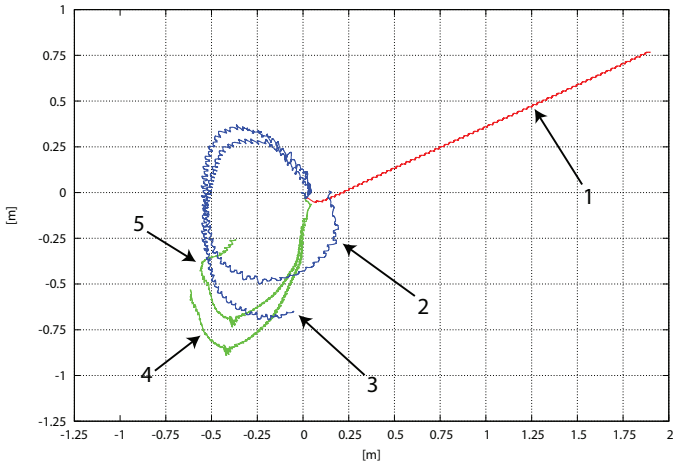

Fig. 9. Trajectories resulting from $60s$ of simulated forward movement (red), left turns (blue), and right turns (green). Initially located at $(0, 0)$, and oriented along the positive x-axis, Annelid's forward movement (1) results from a sinusoidal temperature wave travelling from its head to its tail (cf. Sec. V-A). Note that the robot does not move in parallel to the x-axis due to currently uncontrolled friction while initially heating up the robot. Curved movement is triggered by additionally heating up Annelid's skeleton segments that belong to its flanks close to the center of curvature (cf. Sec. V-B). It holds $\delta E = 0J$ for (3,4), and $\delta E = -2.5J$ for (2,5) in the computation of $E(flankSeg)$ in (6).

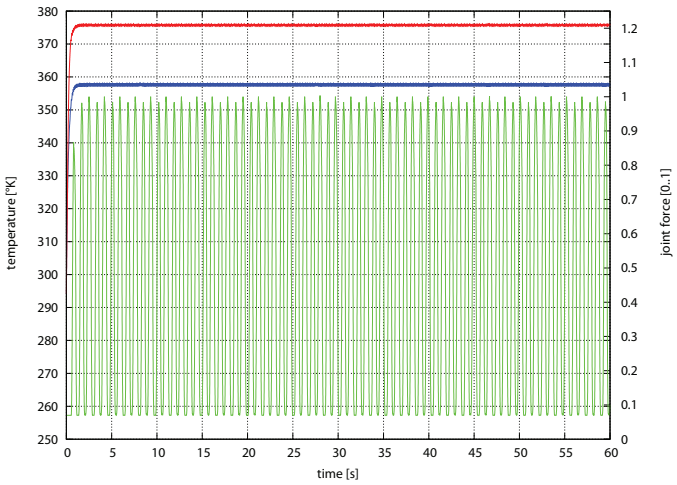

Fig. 10. Minimal (blue) and maximal (red) temperature of Annelid's skeleton during $60s$ of simulated forward movement as depicted in trajectory 1 in Fig. 9. The green curve depicts the normalized force exerted by an arbitrary but fixed chosen joint connecting two consecutive skeleton segments.

VI. Conclusions and Future Work

In this work we have presented a novel design for snake-like robots, based on a spring-style skeleton made of SMA. The main contribution of this paper is given by a feasibility study in terms of a simulation framework that addresses constructional details such as the modeling of the skeletons's spring-like behavior, the description of a prestressing flexible skin, and a thermodynamic simulation of the heating- and cooling-mechanism involved.

Simulation results show that the proposed design can produce stable forward movement, as well as trajectories with controlable curvature.

A. Future Work

The next upcoming step in the realization of the presented ideas is to set up a physical workbench version of Annelid. In this configuration we have to approve the feasibility of the presented heating and cooling mechanism under several aspects. First we have to assure the controlability of the skeleton's thermal energy within a tight range of operation, since overheating may permanently damage the SMA's Austensite effect. A second task that will be investigated with this mock-up, is the selection of an appropriate material for Annelid's skin. According to our presented simulation results, this material must at least resist to, and isolate from, skeleton temperatures of around $100°C$. This requirement is hard, since we need a huge temperature difference between the skeleton and the cooling air in order to dissipate thermal energy fast enough.

Acknowledgment

This work has been partially funded by the Deutsche Forschungsgemeinschaft in the context of the SFB/TR8 "Spatial Cognition".

References

[1] Z. Bo and D. Lagoudas. Thermomechanical Modeling of PolycrystallineSMAs under Cyclic Loading, Part I: theoretical derivations. *International Journal of Engineering Science*, 37(9):1089–1140, 1999.

[2] S.M. Dutta and F.H. Ghorbel. Differential Hysteresis Modelling of a Shape Memory Alloy Wire Actuator. *IEEE Transactions on Mechatronics*, 10(2):189–197, 2005.

[3] C.A. Edwards and P.J. Bohlen. *Biology and Ecology of Earthworms*. Chapman & Hall, 3^{rd} edition, 1996.

[4] I. Erkmen, A.M. Erkmen, F. Matsuno, R. Chatterjee, and T. Kamegawa. Snake robots to the rescue! *IEEE Robotics & Automation Magazine*, 9(3):17–25, 2002.

[5] J.K. Hopkins, B.W. Spranklin, and S.K. Gupta. A survey of snake-inspired robot designs. *Bioinspiration & Biomimetics*, 4(2), 2009. DOI: 10.1088/1748-3182/4/2/021001.

[6] A. Menciassi, D. Accoto, and S. Gorini. Development of a biomimetic miniature robotic crawler. *Autonomous Robots*, 21:155–163, 2006.

[7] R.R. Murphy. Trial by fire – activities of the rescue robots at the world trade center from 11-21 september 2001. *Robotics and Automation Magazine*, 11(3):50 – 61, 2004.

[8] NVIDIA Corporation, 2701 San Thomas Expressway Santa Clara, CA 95050, USA. NVIDIA PhysX for Developers, 2010. `http://developer.nvidia.com/object/physx.html`.

[9] K. Otsuka and C.M. Wayman, editors. *Shape Memory Materials*. Cambridge University Press, 2002.

[10] SAES Getters, Viale Italia 77, 20020 Lainate (Milan), Italy. SmartFlex Compression and Tensile Springs, 2010. `http://www.saesgetters.com/documents/compression%20and%20tensile%20springs%20datasheets_low_1487.pdf`.

[11] SAES Getters, Viale Italia 77, 20020 Lainate (Milan), Italy. SmartFlex Wire Product Datasheet, 2010. `http://www.saesgetters.com/documents/smartflexproductdatasheet_low_1486.pdf`.

[12] N.Ma. Song and H-J. Lee. Position control of shape memory alloy actuators with internal electrical resistance feedback using neural networks. *Smart Materials and Structures*, 13:777–783, 2004.

[13] H. Stöcker. *Taschenbuch der Physik*. Harri Deutsch Verlag, Frankfurt am Main, Germany, 2010.

[14] J. Sui, Z. Gao, H. Yu, Z. Zhang, and W. Cai. Martensitic and magnetic transformations of $Ni_{56}Fe_{17}Ga_{27-x}Co_x$ high-temperature ferromagnetic shape memory alloys. *Scripta Materiala*, 59(8):874–877, 2008.

[15] Z. Zhu, J. Wang, and J. Xu . Modeling of Shape Memory Alloy Based on Hysteretic Nonlinear Theory. *Applied Mechanics and Materials*, 44–47:537–541, 2011.